

Synergistic Interface Platforms: Designing Superhydrophilic Conductive Nanoparticle-Decorated Nanofibrous Membranes

Antonios Keirouz, Ute Jungwirth, Arthur Graf, and Hannah S. Leese*


In today's technological landscape, advancing methods for producing conductive membranes that simplify and streamline the development of advanced interface materials is crucial. This study introduces a versatile and innovative method for fabricating superhydrophilic, conductive nanofibrous membranes based on the in situ synthesis of polypyrrole nanoparticles on poly(vinylidene fluoride-co-hexafluoropropylene) (PVDF-HFP) electrospun fibers. The composite membranes morphologically exhibit a particle-decorated nanofibrous configuration, with polypyrrole nanoparticles distributed along the individual fibers' surface. The nanoparticle-nanofiber configuration shows distinctive properties; electrochemically, the electrospun mats demonstrate excellent inherent electrical conductivity, good cyclic and high electrochemical stability, and low resistance. Furthermore, the amphiphilic and superhydrophilic behavior, achieved through nanotopography, porosity and interactions between the intrinsically conductive polymer and the PVDF-HFP fibers, enables efficient uptake of polar and nonpolar analytes. The membranes also demonstrate good in vitro cell viability of both murine and human fibroblasts. Given its efficient interaction with liquids and omnidirectional 360-degree conductivity, this material emerges as an excellent candidate for use as a biocompatible, multifunctional interface layer. The produced nanoparticle-nanofibrous membrane materials offer a promising platform for interface applications, featuring enhanced spatiotemporal configurations and wide-ranging applicability.

1. Introduction

Polymeric multifunctional membranes that synergistically combine conductivity and superhydrophilicity hold significant promise for advancements across diverse fields. In electrochemical sensing, an amphiphilic conductive membrane can promote the efficient transport of analytes, enhancing sensitivity and sensor response time.^[1] In the pursuit of a sustainable energy economy and the quest for metal-free photocatalysts and energy storage devices, such a polymeric membrane can enhance the performance of batteries and supercapacitors by facilitating efficient ion transport and improving charge/discharge rates.^[2,3] The rapid water transport through a superhydrophilic membrane, coupled with the ability to apply an electrical potential, could be used to control separation processes^[4] and enhance antifouling properties.^[5] In the field of tissue engineering, conductive membranes can enhance bone tissue regeneration,^[6] while the combination of

A. Keirouz, H. S. Leese
Materials for Health Lab, Department of Chemical Engineering
University of Bath
Bath BA2 7AY, UK
E-mail: h.s.leese@bath.ac.uk

A. Keirouz, H. S. Leese
Centre for Bioengineering and Biomedical Technologies (CBio)
University of Bath
Bath BA2 7AY, UK

 The ORCID identification number(s) for the author(s) of this article can be found under <https://doi.org/10.1002/admi.202400040>

© 2024 The Authors. Advanced Materials Interfaces published by Wiley-VCH GmbH. This is an open access article under the terms of the [Creative Commons Attribution](#) License, which permits use, distribution and reproduction in any medium, provided the original work is properly cited.

DOI: 10.1002/admi.202400040

U. Jungwirth
Department of Life Sciences
University of Bath
Bath BA2 7AY, UK

U. Jungwirth
Translational and Clinical Research Institute
Newcastle Drug Discovery Group
Newcastle University
Paul O'Gorman Building, Newcastle upon Tyne NE2 4HH, UK

A. Graf
HarwellXPS
Research Complex at Harwell
Rutherford Appleton Lab
Didcot OX11 0FA, UK

A. Graf
School of Chemistry
Cardiff University
Main Building, Park Place, Cardiff CF10 3AT, UK

superhydrophilicity and conductivity can find applications in functional tissue constructs and antimicrobial wound dressings by facilitating cell adhesion, proliferation, and cell differentiation.^[7] As such, focusing on developing multifunctional membranes with synergetic surface properties holds the potential for exciting advancements in energy, environmental, and biomedical applications.

Electrospinning exploits electrohydrodynamic phenomena to generate continuous polymeric fibers with diameters ranging from a few nanometers to several micrometers.^[8] The process involves the application of an electric field to a polymer solution, which leads to the formation of a charged jet that is then elongated and solidified into fibers as it travels toward a grounded or oppositely charged collector surface, ultimately discharging them.^[9] Due to their high surface area-to-volume ratio and porous, permeable structure, electrospun membranes can operate as excellent substrates for enhancing binding capacity, particle distribution, and kinetics.^[10] By exploiting this approach to synthesize a conductive polymer layer onto electrospun fibers, the need for a separate interface layer (usually made of metals or metallic coatings) can be eliminated. This simplification reduces the number of steps involved in device development.

Electrospun membranes composed of intrinsically conductive polymers (ICPs) offer numerous advantages compared to incorporating metals or metallic coatings into the polymeric matrix due to nanoscale effects, including enhanced reactivity, tunability of conductivity, metal-free composition, and flexibility in structural modification.^[11] The high surface area and porosity of electrospun membranes can augment the distribution and growth of the ICP along the fibers' surface, thereby improving the number of accessible active sites and facilitating efficient charge transfer and ion transport.^[12] Additionally, ICPs possess the ability to switch between different oxidation states, leading to changes in properties such as conductivity, magnetism, and chemical responsiveness.^[13] This tunability can enable the introduction and optimization of electrical conductivity via the synthesis of ICP onto non-conductive electrospun membranes that exhibit chemical resistance and thermal stability.

In this work, we present an adaptable method for fabricating conductive polypyrrole (PPy) particles directly on poly(vinylidene fluoride-co-hexafluoropropylene) (PVDF-HFP) electrospun membranes. PVDF-HFP, a well-established polymer in membrane preparation, was chosen for its excellent electrospinnability, thermal stability, and advantageous properties, including high dielectric strength and resistance to chemicals, solvents, and UV radiation.^[14,15] Additionally, the presence of strong carbon-fluorine bonds in the polymer chain makes it chemically inert and highly resistant to chemical attack (including acids) and degradation, thereby rendering it an ideal candidate to act as a substrate for chemical oxidative polymerization.^[14,15] The selection of PPy as the ICP was driven by its excellent electrical conductivity, electrochemical properties, and electrically responsive behavior, which can enhance the overall performance of such membranes.^[16,17] PPy can be synthesized on a large scale in an environmentally friendly and cost-effective manner, and it is associated with low temperature processability and high electrocatalytic properties.^[18] The produced nanoparticle-nanofiber membranes were thoroughly assessed through morphological analysis, chemical characterization, wettability evalua-

tion, thermal analysis, biocompatibility testing, and electrochemical performance evaluation to determine the composite's unique properties.

2. Results and Discussion

Initially, PVDF-HFP nanofibrous membranes were produced via electrospinning. Subsequently, the membranes were used as a substrate for the in situ synthesis of polypyrrole (PPy) through chemical oxidative polymerization in the presence of pyrrole (monomer) using iron chloride hexahydrate (oxidizing agent) (Figure 1a). The successful synthesis of PPy onto the electrospun membranes was initially realized by a color change from white (representing pristine PVDF-HFP) to black (representing PVDF-HFP-PPy). This observation was further confirmed by submerging PVDF-HFP membranes, which had not been pre-embedded in pyrrole, directly into the oxidizing solution, where no color change was observed under the same polymerization conditions (Figure S1, Supporting Information).

2.1. Morphological Observations

The micromorphology and corresponding fiber diameter distribution plots of the electrospun nanofibers (NFs) are presented in the scanning electron micrographs (Figure 1b; Figure S2, Supporting Information). The SEM analysis reveals that all the produced membranes exhibit a consistent fiber morphology, devoid of beads or significant secondary defects, and display a randomized fibrous matrix architecture. The pristine PVDF-HFP NFs exhibit a smooth surface with an average fiber diameter of 168 ± 74 nm. The composite PVDF-HFP-PPy membranes display a particle-decorated configuration, wherein individual fibers appear adorned with PPy nanoparticles (NPs). The composite membrane demonstrates a randomly-oriented matrix of curved fibers (average fiber diameter 248 ± 97 nm) with PPy particles distributed along the fibers' surface (average particle diameter 309 ± 146 nm). During polymerization, the average fiber diameter of the pristine PVDF-HFP membranes increased by $\approx 50\%$, due to the growth of PPy chains along the surface of the pristine fibers. This increase in diameter was further supported by the observation that the PVDF-HFP-PPy membranes, following the synthesis, washing, and drying processes, exhibited a weight increase of $235\% \pm 27\%$ compared to the pristine PVDF-HFP membranes. As the particle distribution on the fibers depends on the substrate area during polymerization, the area was controlled by cutting the pristine PVDF-HFP membranes into predetermined dimensions and maintaining consistent oxidizing conditions (depicted in the photographs in Figure 1a; Figure S1, Supporting Information).

Cross-sectional imaging reveal a markedly roughened fiber surface in the hybrid PVDF-HFP-PPy membranes (Figure 1c; Figure S6, Supporting Information) compared to pristine PVDF-HFP (Figure S7, Supporting Information). This morphology is indicative of the in situ coating of the electrospun membrane's internal structure, likely facilitated by the inherent porosity of the material. The observed morphology aligns with the proposition of PPy preferentially growing on the individual PVDF-HFP fibers. Qualitative analysis of the hybrid fibers' cross-section suggests a 60–80 nm surface coating, which is consistent with the

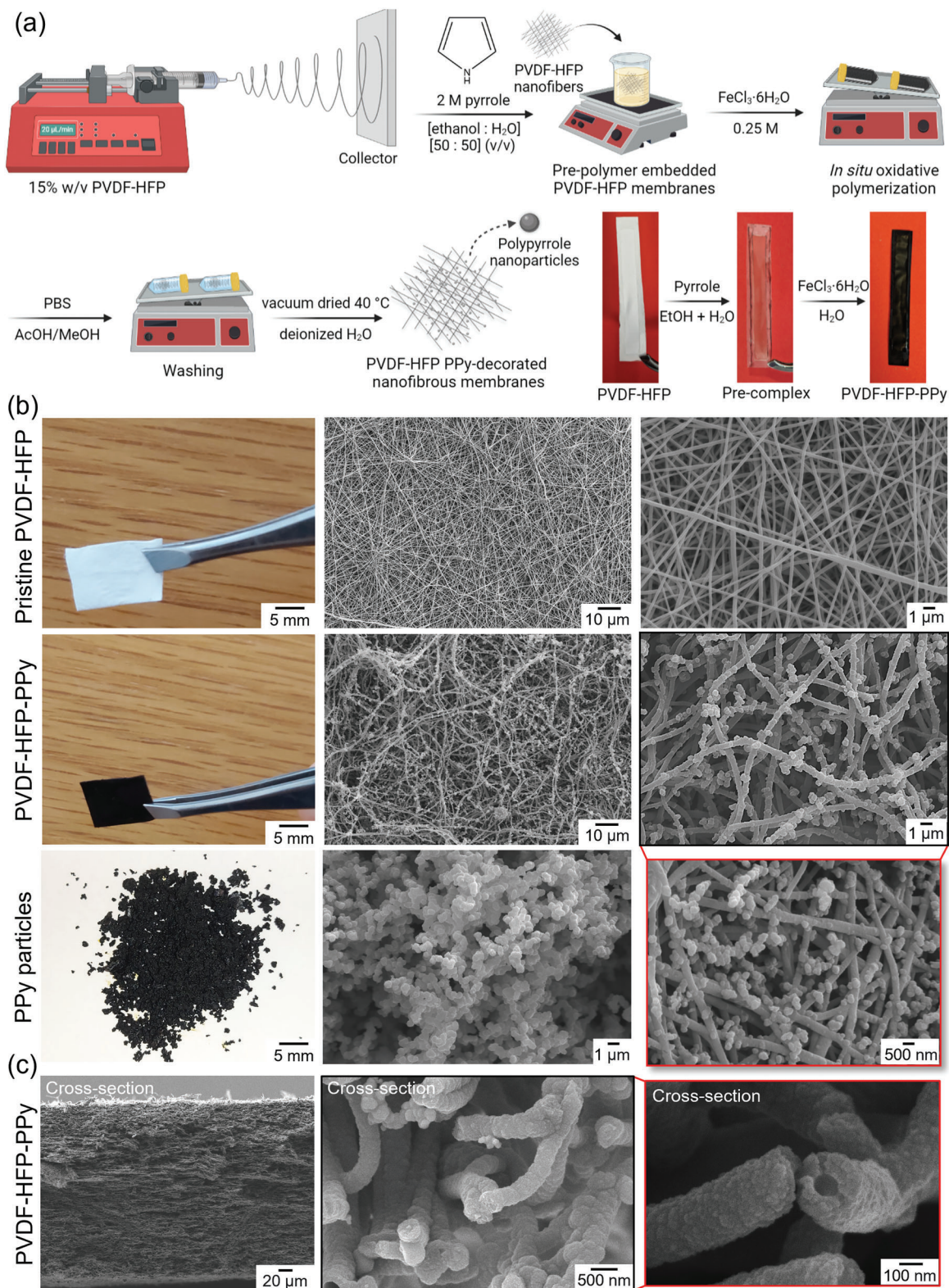


Figure 1. Fabrication protocol of PPy particle-decorated PVDF-HFP electrospun membranes. a) Schematic representation of the in situ synthesis process. b) Photographs and SEM micrographs displaying the pristine PVDF-HFP, composite PVDF-HFP-PPy electrospun membranes, and pristine PPy particles, with a magnified region of the PVDF-HFP-PPy highlighted in red. c) Cross-section SEM micrographs of the hybrid PVDF-HFP-PPy membranes, with a cross-sectional magnification of a single PVDF-HFP-PPy fiber highlighted in red. Created using BioRender.

reported increase in fiber thickness. Notably, the thickness of the membranes did not change significantly between the two groups (ranging between 200–240 μm). The increase in fiber thickness was accompanied by a corresponding increase in average pore size, as evidenced by the mean flow pore size. The pristine PVDF-HFP membranes (Figure S3, Supporting Information) exhibited a mean pore size of 0.70 μm , whereas the composite PVDF-HFP-PPy membranes (Figure S4, Supporting Information) exhibited an increase to 1.11 μm .

To further assess the stability of the PPy nanoparticles on the electrospun NFs, the composite membranes were exposed to constant magnetic stirring (500 rpm) in distilled water for 24 h, followed by 30 min of sonication. Notably, no observable morphological variations were detected in terms of the distribution or the absence of the PPy NPs on the fiber surface following washing (see Figure S5, Supporting Information). This finding was further supported by four-point probe measurements, which demonstrated no significant change ($p > 0.05$) in membrane resistance before ($0.57 \pm 0.04 \Omega \text{ sq}^{-1}$) and after ($0.58 \pm 0.1 \Omega \text{ sq}^{-1}$) undergoing thorough washing, thus indicating a certain degree of stability (as shown in Table S1, Supporting Information).

During the chemical oxidative polymerization of pyrrole, the dopant used can determine the charge state of the PPy particles.^[19] If a positively charged dopant, such as an acid (in this work, iron chloride hexahydrate) or protonating agent, is used, the PPy particles will carry a positive charge PPy^+ .^[20] Although the substrate used for the in situ synthesis, PVDF-HFP, is a non-conductive polymer, and its surface is generally considered electrically neutral, it contains a high proportion of the most electronegative element, fluorine.^[21,22] Due to this, PVDF-HFP can form hydrogen bonds, dipole-dipole interactions, and Van der Waals forces (including London dispersion forces) when interacting with other polar substances.^[23,24] Additionally, the extended π -conjugation and aromatic character of the PPy particles can promote π - π stacking interactions along the PVDF-HFP surface.^[25] The combination of π - π stacking interactions among the PPy particles and the surrounding non-covalent interactions between PPy and PVDF-HFP can contribute to the overall stability and integrity of the PPy particles decorating the individual PVDF-HFP NFs.

2.2. Superhydrophilic Behavior of the PPy-Decorated Electrospun Membranes

Along with the membrane's morphological characteristics, the material surface properties can influence the strength and distribution of charges. In our case, PVDF-HFP is inherently hydrophobic, while PPy hydrophilic. These contrasting surface properties can further facilitate interactions that help anchor the PPy particles onto the surface of the PVDF-HFP fibers, preventing the detachment of particles. The pristine PVDF-HFP NFs exhibited a water contact angle (WCA) of $136^\circ \pm 7^\circ$, consistent with the reported values for electrospun membranes in the literature.^[26,27] However, the presence of PPy NPs along the surface of PVDF-HFP membranes dramatically reduced the WCA of the pristine nanofibrous membranes to 0° instantaneously (Figure 2a). This change in wettability properties is visually demonstrated in Video S1 (Supporting Information), which

presents a compilation of measurements comparing the pristine PVDF-HFP membranes to the composite PVDF-HFP-PPy membranes. PPy is hydrophilic, as demonstrated in our work, when synthesized on top of a flat acrylic surface, presenting a WCA of $62^\circ \pm 6^\circ$, in agreement with previously published work.^[28] Here, the PPy particles effectively incorporated along the nanofibrous configuration enhance the wetting properties of hydrophobic electrospun polymeric membranes.

Superhydrophilic substrates, characterized by a large surface area and the presence of functional groups and free radicals that exhibit ultra-strong affinity for binding water molecules, effectively suppress the surface tension of water.^[29] This reduction in surface tension leads to a WCA of 5 – 10° or allows for the complete absorption of water across the substrate's surface.^[30] The -NH functional groups on the membrane surface, facilitated by the presence of the PPy particles, contribute to the formation of hydrogen bonds with water molecules, effectively entrapping them. Furthermore, previous research on the topic has demonstrated that increasing the pore size of a material, including electrospun membranes, can enhance its hydrophilicity and vice versa.^[31,32] We determined that each composite membrane could absorb an amount of water equal to $314\% \pm 16\%$ of its initial weight, as opposed to $108 \pm 8\%$ for the pristine PVDF-HFP membranes.

In contrast to our findings, Aguiar et al.^[33] employed a similar methodology for the in situ synthesis of polypyrrole using polystyrene electrospun membranes (WCA $105^\circ \pm 2^\circ$). They observed that the deposition of polypyrrole chains on the surface of the fibers did not alter the composite material's WCA (WCA $105^\circ \pm 3^\circ$). However, they achieved a superhydrophilic surface by subjecting the composite to plasma treatment at 300 mTorr for 5 min. In their work, the composite membranes presented a smaller quantity of PPy particles along the surface of thicker fibers ($\approx 1 \mu\text{m}$ in diameter), while the fiber diameter did not vary between the pristine and composite fibers. Furthermore, their synthesis process involved polymerizing the fibers in ferric chloride using a concentration of 0.48 mM of pyrrole, in contrast to our study, which utilized a concentration of 1.8 M.

Another study by Číková et al.^[34] demonstrated that the choice of oxidizing agent influences the hydrophilicity of polypyrrole. They found that the incorporation of an anionic surfactant (dodecylbenzenesulfonic acid) when pyrrole is polymerized in the presence of FeCl_3 could reverse the hydrophilic nature of the substrate, resulting in the production of hydrophobic (WCA $115^\circ \pm 4^\circ$) polycaprolactone-PPy electrospun membranes. Thus, there exists a threshold that considers the quantity of PPy attached to the electrospun membranes, the particle size, and the conditions of oxidation during synthesis, all of which collectively impact the surface energy and water affinity of the composite end product.

To gain further insight into the composite membrane's affinity toward oil, the oil contact angle (OCA) of both the PVDF-HFP and PVDF-HFP-PPy electrospun membranes was evaluated. The pristine PVDF-HFP membrane exhibited an OCA of $23^\circ \pm 1.4^\circ$, while the incorporation of PPy into the PVDF-HFP structure notably enhanced its oleophilic properties, resulting in a significantly reduced OCA ($p \leq 0.001$) of 0° (Figure S6 and Video S2, Supporting Information). This observation suggests that the produced composite electrospun membranes exhibit amphiphilic behavior, which favors polar and nonpolar substrates.

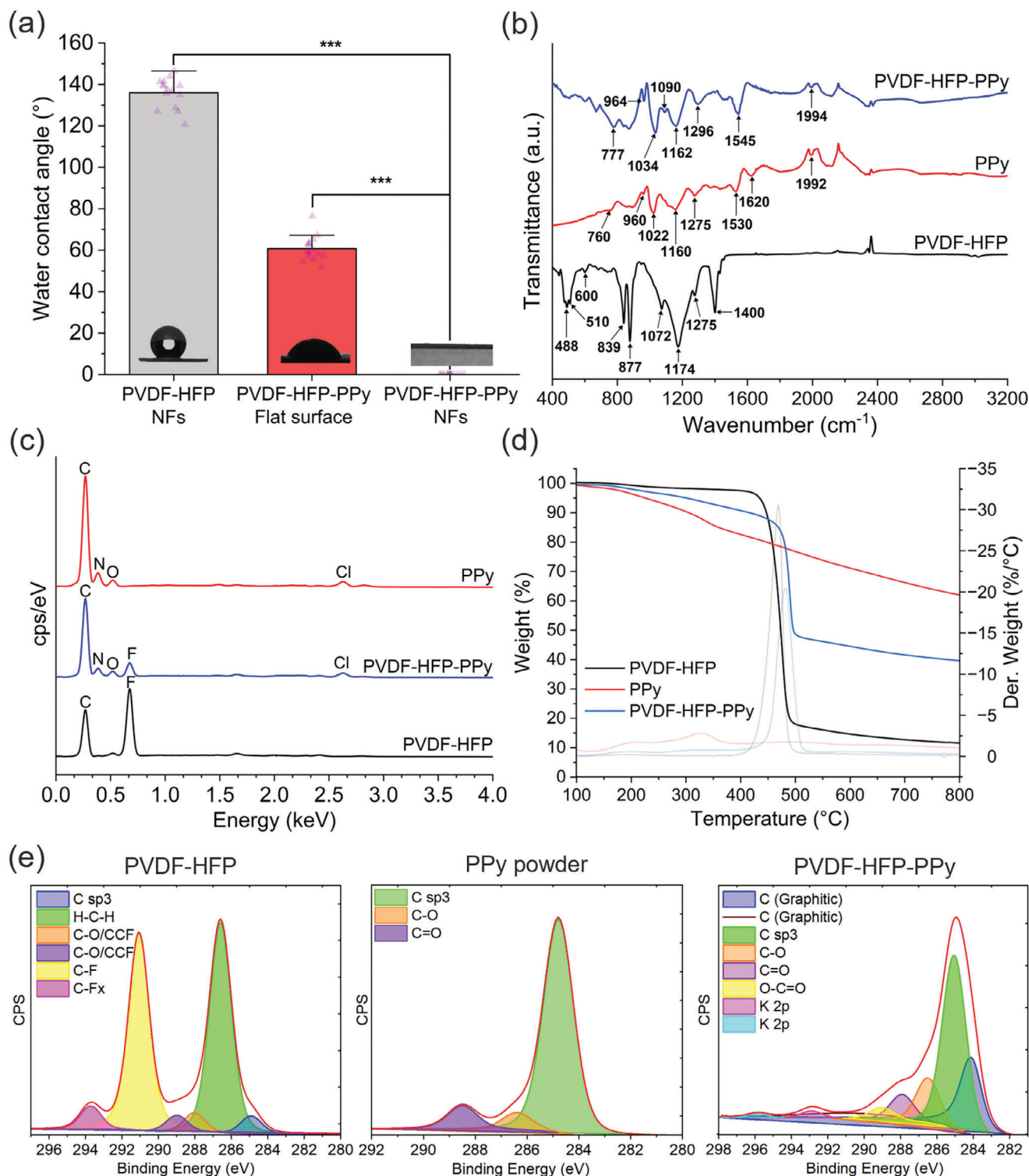


Figure 2. Chemical analysis of the electrospun membranes and polypyrrole (PPy) nanoparticles confirms successful PPy synthesis onto PVDF-HFP. a) Water contact angle (WCA) measurements. Static water contact angle measurements were conducted on the pristine nanofibers (NFs), a flat-coated surface, and the composite NFs. The data are presented as mean \pm SD, with $n = 8$ replicates. Statistical significance was determined using Student's t-test: *** $p \leq 0.001$. b) ATR-FTIR spectra comparing the pristine and composite electrospun membranes. c) Representative graphs depicting energy-dispersive X-ray (EDX) elemental mapping. d) Representative thermogravimetric analysis with derivative weight. e) X-ray photoelectron spectroscopy (XPS) analysis of the carbon C1s binding energies.

Consequently, these membranes can effectively interact with and attract both oil and water molecules.

The particles stability on the electrospun nanofibrous membranes and the observed superhydrophilic behavior stems from a complex and multifaceted interplay of events involving the chemistry of the two polymers, as well as enhanced capillary forces due to the increased surface area, porosity, and high fiber density provided by the electrospun nanostructure.^[34] These factors potentially synergize to augment interactions with water molecules and facilitate superior wettability by promoting increased capillary action, improved water adsorption capacity, and facilitated permeance.

2.3. Chemical Characterization and Composition Analysis

FTIR analysis was utilized to determine the chemical composition of the PVDF-HFP NFs, PPy particles and PVDF-HFP-PPy composite electrospun membranes (Figure 2b). The spectra of the constituent materials can be found in Figure S7 (Supporting Information). PVDF-HFP is a copolymer consisting of vinylidene fluoride (VDF) and hexafluoropropylene (HFP) monomers. The FTIR spectrum of the PVDF-HFP NFs presents significant peaks at 1400, 1275, 1174, 1072, 877, 839, 600, 510, and 488 cm^{-1} . The absorption bands at 600, 510, 488 cm^{-1} and 1037, 964, and 777 cm^{-1} can be assigned to the α -phase and β -phase of PVDF-HFP, respectively. The peaks at 1275, 1174, and 1072 cm^{-1} are associated with the bending and wagging vibrations of CF bonds in the HFP and VDF units. The peak at 1400 cm^{-1} can be attributed to the in-plane bending of the CH_2 in the α -phase. This interpretation agrees with previously published works.^[35–37]

The presence of PPy is confirmed by the observed absorption bands at 1992, 1530, and 1620 cm^{-1} (corresponding to C = C and C-C stretching modes of the pyrrole ring), the secondary heterocyclic amine at $\approx 1275 \text{ cm}^{-1}$ (attributed to the C-N stretching mode of the pyrrole ring), and the breathing C-H bipolaron vibration bands of the pyrrole rings at 1160 and 1022 cm^{-1} . Peaks below 1000 cm^{-1} indicate skeletal vibrations of the polymer. The observed peaks align closely with the findings from prior studies.^[38] Notably, the FTIR spectrum of the composite PVDF-HFP-PPy structure exhibits predominately characteristic absorption bands of the PPy structure, indicative of its presence at the surface of the NFs.

To further confirm the presence of PPy in the composite membranes, energy dispersive X-ray spectroscopy (EDX) elemental maps and X-ray photoelectron spectroscopy (XPS) were obtained for the PPy particles, PVDF-HFP, and PVDF-HFP-PPy membranes (Figure 2c,e). The EDX elemental analysis revealed additional populations of N, along with C and F, distinct from the presence of PPy in the composite structure. In contrast, the pristine PVDF-HFP membranes only exhibited C and F. The quantitative contents and theoretical values of the constituent compounds are summarized in Table 1. The atomic percentages of the elements align with the theoretical amounts specified for each compound, providing additional evidence for the presence of in situ synthesized PPy on top of the PVDF-HFP NFs. The small amounts of Cl anions indicate the PPy synthesis route involving ferric chloride, while the absence of Fe results from the meticulous washing methodology employed.

Table 1. EDX elemental analysis of PVDF-HFP NFs, PPy NPs, and PVDF-HFP-PPy NFs specimens. The distinctive elements reasserting the synthesis of PPy onto the PVDF-HFP electrospun membranes are highlighted in yellow ($n = 3$). The values represent the average \pm SD of each element.

PVDF-HFP NFs	
Element (K-line)	Atom%
C	51.4 \pm 3.4 (50)
F	48.6 \pm 3.5 (50)
PPy NPs	
Element (K-line)	Atom%
C	76.0 \pm 3.1 (80)
N	19.2 \pm 3.1 (20)
O	4.8 \pm 0.3
PVDF-HFP-PPy NFs	
Element (K-line)	Atom%
C	58.5 \pm 2.9
F	25.2 \pm 2.5
N	12.3 \pm 0.8
O	4.0 \pm 0.7

The percentages in brackets () refer to the theoretical values of PPy and PEDOT:PSS, respectively.

X-ray photoelectron spectroscopy (XPS) revealed distinct surface chemistry between pristine and hybrid membranes (Figure S10, Supporting Information). Quantitative analysis (Table S1, Supporting Information) showed a significant increase in carbon content (70% in PPy powder, 46% in hybrid membranes) compared to the pristine PVDF-HFP NFs, which exhibited a high fluorine concentration (F:C ratio of $\approx 2:1$). This potentially suggests surface enrichment of fluorine during electrospinning, where the electronegative nature of the fluorine might favor its orientation toward the surface of the fibers during elongation and solidification. Notably, the hybrid membranes displayed characteristic oxygen and nitrogen peaks indicative of the presence of PPy, while the absence of detectable fluorine (XPS probing depth $\approx 10 \text{ nm}$) is evidential of the extensive PPy coating of the individual PVDF-HFP fibers.

High-resolution C1s XPS spectra (Figure 2e) reveals that the PPy powder can be deconvoluted into: C-C ($\approx 284.7 \text{ eV}$), C-O/C-X ($\approx 286.4 \text{ eV}$, X = N or Cl), and C = O ($\approx 288.4 \text{ eV}$). PVDF-HFP NFs exhibited a dominant presence of fluorine and carbon (50% and 49.4%, respectively). The C-C/C-N peak ratio suggested potential airborne contamination, evidenced by adventitious carbon (C 1s < 1%). Oxygen appears as a minor contribution, with less than 1%. Peaks corresponding to C-F ($\approx 291 \text{ eV}$) and H—C—H bonds ($\approx 286.6 \text{ eV}$) displayed a near 1:1 ratio, consistent with the expected PVDF structure. Multiple fluorine environments were identified, including C-O/CCF ($\approx 286 \text{ eV}$) and C-Fx ($\approx 293.7 \text{ eV}$). A single chemical environment was observed for both O 1s and F 1s (Figures S11 and S12, Supporting Information).

In contrast, the C1s spectrum for the hybrid PVDF-HFP-PPy membranes is more intricate, requiring multiple peaks for accurate fitting. A prominent feature was the asymmetric peak at $\approx 284.1 \text{ eV}$ indicative of graphitic carbon. Additional components

included C sp³ (285 eV), C-O/C-X (286.5 eV), C = O (287.9 eV), and O-C = O (289 eV). Notably, K 2p peaks were observed at higher binding energies (≈ 293 and ≈ 296 eV).

Thermogravimetric analysis (TGA) was conducted to assess the composite structure's thermal stability and decomposition behavior under an argon atmosphere (Figure 2d). Three groups were investigated: PPy particles, PVDF-HFP, and PVDF-HFP-PPy NFs. The weight loss of all groups was found to be less than 4% (less than 2% for the electrospun membranes) at temperatures below 200 °C, indicating that the membranes and particles were adequately dried with minimal residual solvent or moisture entrapment.

The PVDF-HFP electrospun membranes exhibited an initial decomposition starting at ≈ 400 °C and completing at ≈ 500 °C. This decomposition of the polymer backbone resulted in the formation of gaseous byproducts such as hydrogen fluoride and vinylidene fluoride, accounting for an 80% weight loss. The derivative curve of the TGA analysis showed a distinct peak at 470 °C, indicating a sharp decomposition process. The PPy powder displayed a continuous decomposition/degradation pattern, with a gradual weight loss as the temperature increased, without reaching a plateau. A more defined steep decline in weight loss was observed after 180 °C, accounting for $\approx 40\%$ weight loss by 800 °C.

In the case of the PVDF-HFP-PPy composite structure, the TGA curve exhibited an intermediate weight loss behavior, falling between the weight loss behaviors observed for the pristine PVDF-HFP membranes and the PPy particles. This suggests that the presence of PPy in the composite structure influenced the thermal decomposition behavior of the PVDF-HFP.

The composite structure showed a similar decline in weight loss as the PPy particles up until ≈ 440 °C, where it exhibited a conceptually similar steep decomposition attributed to the PVDF-HFP membrane. However, the weight loss of the composite structure accounted for 60% by 800 °C, compared to 90% for the PVDF-HFP pristine membranes. This indicates that the growth of PPy along the PVDF-HFP electrospun membranes contributes significantly to the weight proportion of the composite structure, influencing the thermal decomposition behavior of the PVDF-HFP membrane. This agrees with the fact that the composite membranes presented \approx a 93% weight increase (dried) than the pristine membranes. The derivative peak of the composite structure's TGA curve shifted at 182 °C, possibly due to the higher melting point of pyrrole ($T_m > 300$ °C) compared to PVDF-HFP (T_m 160–170 °C). The observation that the composite structure exhibited a lower weight loss percentage (60%) than pristine PVDF-HFP membranes (90%) suggests that the presence of PPy influenced the thermal stability of the PVDF-HFP membrane, possibly by contributing to the composite's thermal insulation or altering decomposition pathways. This could be due to the presence of conductive PPy particles, which may affect the heat dissipation of the composite structure. However, the most likely reason is that the distribution of the two polymers could influence the overall thermal behavior. The presented results seem to align with known trends in the literature for PVDF-HFP and PPy and additionally provide some first-reported insights into the thermal behavior of the composite.

2.4. Assessing the Electrochemical Performance of Composite Membranes

The electrical and electrochemical performance and stability of the composite PVDF-HFP-PPy electrospun membranes were assessed to elucidate their electrochemical behavior. Cyclic voltammetry (CV) was performed to provide mechanistic information regarding the flow of electrons within the composite structure and to determine any changes in electron transfer.

The qualitative electrical and electrochemical performance of the composite membranes is presented in Figure 3. The cyclic voltammograms depict the stability of the PVDF-HFP-PPy membranes over a period of 100 cycles within the supporting phosphate-buffered saline (PBS) electrolyte. The scan rate was set at 100 mV s⁻¹ with a step potential of 0.01 V. The assessment evaluated the performance and stability of the membranes before (Figure 3a) and after (Figure 3b) being subjected to 24 h of magnetic stirring in deionized water and 30 min of sonication to provide insights into the membrane's ability to maintain its electrical performance. The membrane electrochemical surface area was calculated using the trapezoidal rule applied to the integrated area under the cyclic voltammograms, and it was found to be 0.108 C s (before washing) and 0.107 C s (after washing).

In CV, a symmetric voltammogram with an auroral oval shape between the anodic and cathodic regimes is characteristic of a capacitive behavior of non-Faradaic pseudocapacitive nature.^[39,40] This shape suggests that the material undergoes fast redox reactions over the electrode's exposed area to the electrolyte.^[39] The symmetric shape of the cyclic voltammogram indicates that the material possesses good electrochemical properties and can efficiently store and release electrical energy.^[40] The minimal decline and good overlap observed in both groups over the 100-cycle period can indicate minimal capacity loss.^[41] This suggests that the composite membrane exhibits good cyclic stability. Moreover, the fact that the membranes exhibited similar cyclic voltammograms and current ranges after being subjected to further washing indicates improved capacity retention, high electrochemical stability, and durability.

By varying the scan rate during CV, the electrochemical properties and kinetics of the composite membranes were assessed (Figure 3d). Cyclic voltammograms were obtained for each scan rate within the potential range of 1.5 to -1.5 V (start and stop potential of 0 V) versus Ag/AgCl (reference electrode) at scan rates ranging from 500 to 5 mV s⁻¹. The relationship between scan rate and current intensity provides insights into the stability and electrochemical kinetics of the composite membranes. The results demonstrate an increase in current with incremental increases in the scan rate, indicating rapid electronic and ionic transport rates within the composite membrane. The increased current intensity with increasing scan rate is due to the capacitive effect and reflects pseudocapacitive behavior.^[42] Hussain et al.^[43] demonstrated that the peak-to-peak separations increase significantly with increasing scan rate, indicating quasi-reversible kinetics. Saravanakumar et al.^[44] stated that at higher scan rates, the surface of the active material might not be completely accessed by ions, limiting the diffusion of electrolyte ions. This can result in a higher current due to the collection of ions on the outermost

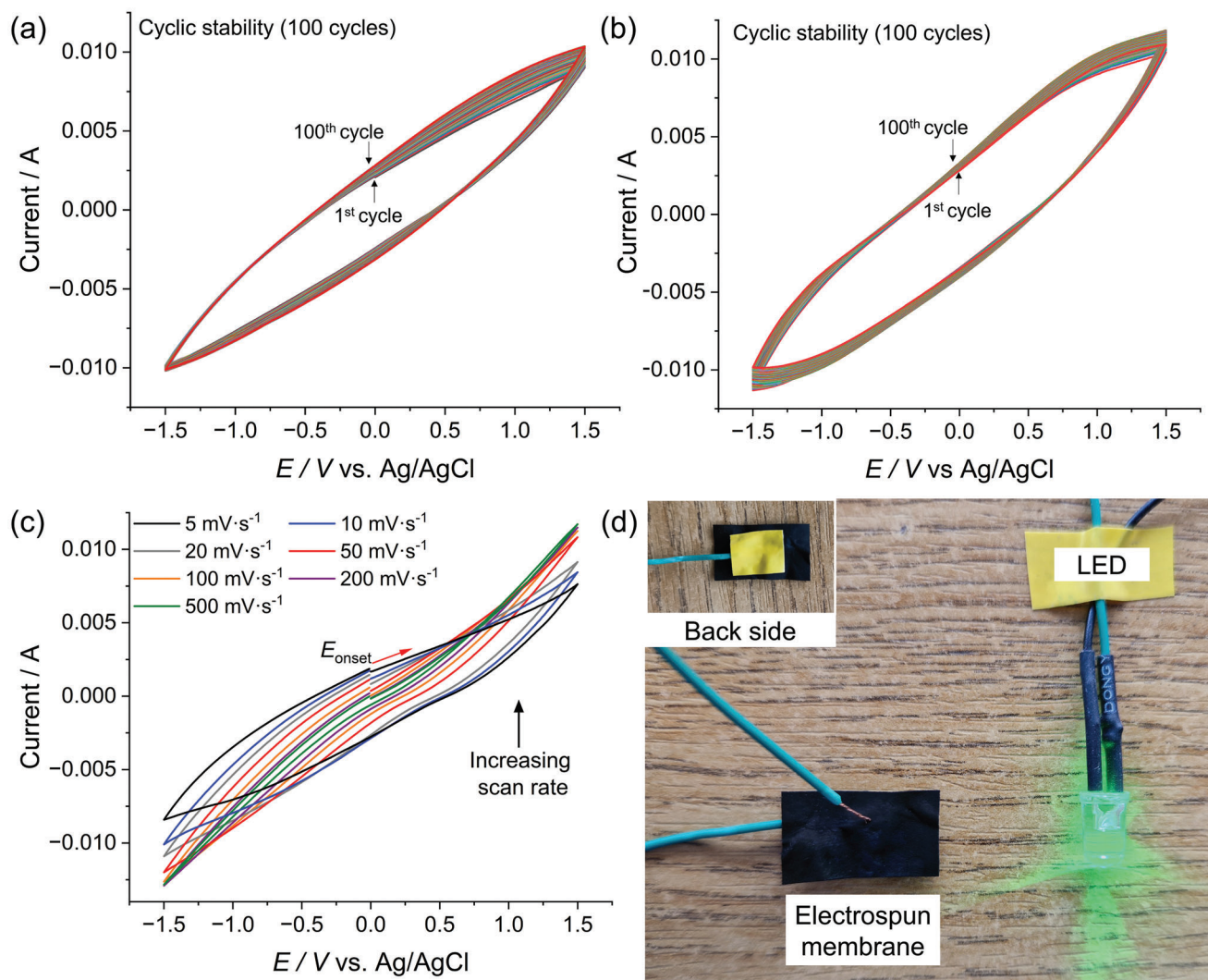


Figure 3. Qualitative analysis of the electrochemical properties and stability of the composite electrospun membranes. a,b) Evaluation of the stability of the nanofibrous membranes before and after subjecting them to 24 h of constant magnetic stirring in phosphate-buffered saline (PBS) pH 7.2 and 30 min of ultrasonication. Cyclic voltammograms of 100 cycles in PBS 7.2, with a scan rate of 100 mV s⁻¹ and a step potential of 0.01 V. The different colors in the cyclic voltammograms represent distinct cycles, highlighting the cyclic nature of the stability examination. Colors do not convey specific information but indicate separate cycles within the analysis. c) Cyclic voltammograms obtained at scan rates of 500, 200, 100, 50, 20, 10, and 5 mV s⁻¹. In both cases, CV measurements were recorded in the potential range of 1.5 to -1.5 V (start and stop potential of 0 V) versus Ag/AgCl (reference electrode), using a Pt wire as the counter electrode. E_{onset} refers to the onset potential. d) Photograph illustrating the capacity of electrospun membranes to function as dry electrodes, illuminating the LED circuit.

surface of the electrode. At the same time, the retention of the shape of the cyclic voltammogram curves at higher scan rates indicates better process reversibility.

The surface conductivity of the dry PVDF-HFP-PPy membranes, measured via four-point probe measurements, was highly conductive at $1.8 \pm 0.35 \text{ S cm}^{-1}$, consistent with previous reports.^[23,45] Polypyrrole is a conductive polymer known for its ability to transport charge and exhibit semiconducting behavior. High conductivity suggests that the composite membranes can efficiently transport electric charge and facilitate the flow of electrons. The successful illumination of the LED indicator (Figure 3d) further substantiates this observation, providing evidence of the PVDF-HFP-PPy mem-

brane's good electrical conductivity and ability to act as a dry electrode.

The ability of the membrane to facilitate the flow of electrons from the 9 V battery to the LED indicates that it can function as an effective conductor in the circuit. As depicted in Video S3 (Supporting Information), the strong brightness and consistent illumination is evidence that the membrane has low resistance and can efficiently transfer charge to the LED, effectively facilitating the redox reactions required to emit light. As the LED remains consistently bright and the illumination does not degrade or fluctuate significantly during contact, it suggests that the membrane is stable and can maintain its conductive properties over time. Additionally, by placing the electrode on the opposite

Table 2. Comparative overview of various conductive electrospun polymer membranes in relation to PVDF-HFP-PPy, spotlighting key parameters including composition, water contact angle (WCA), reported electrical properties, fiber diameter, pore size, and manufacturing approach. NR; not reported.

Composition	WCA [°]	Electrical Properties	Fiber diameter [nm]	Pore size [μm]	Fabrication Method Outline	Refs.
PVDF-HFP-PPy	0	1.80 ± 0.35 (S cm ⁻¹)	248 ± 97	1.11	Chemical oxidative polymerization of PVDF-HFP in the presence of pyrrole	Presented work
PVDF-HFP	136 ± 7	n/a	168 ± 74	0.70	Pristine PVDF-HFP fibers	Presented work
PPy-PCNU	93	776.20 ± 34.08 Ω	270 ± 92	NR	Cryomilled PPy was added to PCNU to achieve a physically-conjugated polymer blend for electrospinning	
PLGA/PDA/CS	0	$2.85 \pm 0.12 \times 10^{-3}$ (S cm ⁻¹)	1379 ± 183	NR	Polydopamine-based coating synthesized via dopamine hydrochloride and adsorbed with chitosan.	
SA/MIL101@PVP-PVDF (4:6 mass)	72	0.237 (S cm ⁻¹)	650	NR	A blended polymeric solution containing 10 wt% SA/MIL-101. Conductivity measurements were obtained at 160 °C at pH 12.7.	
PVDF-C2mpyrFSI-NaFSI	NR	2.60×10^{-3} (S cm ⁻¹)	735	NR	Films were prepared by using a slurry composed of 80 wt% of NaFePO ₄ active material, 10 wt% of PVDF binder and 10 wt% of conductive carbon (cathode films).	
PANi/gelatin	NR	1.84 ± 0.21 (S cm ⁻¹)	154 ± 30	94.66 ± 18.65	Glutaraldehyde crosslinked electrospun PANi gelatin blend.	
T-CA-Nafion	72	0.192 (S cm ⁻¹)	Lost fibrous morphology	n/a	Electrospun membranes produced in the presence of tetrabutylammonium chloride (TBAC) and subsequently cast in Nafion solution.	
T-PA6-Nafion	81.5	0.287 (S cm ⁻¹)	Lost fibrous morphology	n/a		
T-PMIA-Nafion	74	0.225 (S cm ⁻¹)	Lost fibrous morphology	n/a		
PVDF-HFP esHPMEs	NR	3.30×10^{-3} (S cm ⁻¹)	330	NR	Coin cell type Li-ion capacitor with electrospun PVDF-HFP nanofibers. LiCoO ₂ was prepared via solution combustion synthesis.	
PCL/PPy	70–118	0.03 – 9 (S cm ⁻¹)	383-620	NR	Oxidative polymerization of varying amounts of pyrrole in the presence of sodium 2-naphthalenesulfonate (SNS) and FeCl ₃ .	
PCL/PPy	93	$154.90 \pm 0.66 \times 10^{-6}$ (S cm ⁻¹)	200–500	NR	Blended PCL-pyrrole oxidizing solution consisting of DMF:chloroform: FeCl ₃ .	
PVA/mCF@PLA	74 ± 15	3.9×10^4 Ω	Inhomogeneous	NR	Covalently grafted PVA onto mCFs was employed to produce non-woven mats by either dip-coating or electrospinning.	

Abbreviations: PPy-PCNU: polypyrrole-polycarbonate polyurethane; PLGA/PDA/CS: poly(lactide-co-glycolide)/polydopamine/chitosan; SA/MIL101@PVP-PVDF: sulfamic acid (SA)-doped metal-organic framework MIL-101@polyvinylidene fluoride-polyvinylpyrrolidone; PVDF-C2mpyrFSI-NaFSI: PVDF- ionic plastic crystal, N-ethyl-N-methylpyrrolidiniumbis(fluorosulfonyl)imide (C2mpyrFSI) mixed with NaFSI salt; PANi/gelatin: polyaniline/gelatin. T-CA: TBAC- cellulose acetate; T-PA6: nylon-6; T-PMIA: poly-m-phenyleneisophthalamide; EsHPMEs: PVDF-HFP/Li7.1La3Ba0.05Zr1.95O12 nanohybrid membrane electrolytes; PCL/PPy: polycaprolactone-polypyrrole; PVA/mCF@PLA: poly(vinyl alcohol)/ surface-modified carbon nanofibers@poly(lactic acid).

side of the membrane, we were able to further depict the through-out, 360-degree, omnidirectional conductivity of the composite membranes. These findings highlight the potential applications of these interface membranes in electrochemical systems and energy conversion devices.

The performance of the synthesized PVDF-HFP-PPy composite membrane was contextualized within the existing body of research by comparing it to conductive polymeric electrospun membranes recently published in the literature. **Table 2** offers a direct comparison of several key parameters, including material composition, water contact angle (WCA), electrical properties,

(fiber diameter, pore size, of the fabricated PVDF-HFP-PPy composite as well as several electrospun membranes reported in the literature. The PVDF-HFP-PPy electrospun membranes exhibit several desirable properties within the realm of intrinsically conductive polymer-based electrospun membranes. These include superhydrophilicity, porous architecture, and robust cyclic behavior. This distinctive combination of features, which is not present in the reported literature that focuses on electrospun membranes, facilitates the identification of specific strengths and range of applications where this newly developed membrane can be employed.

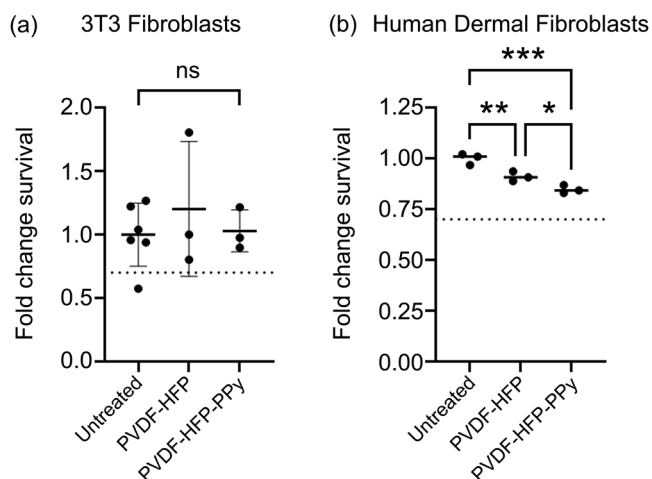


Figure 4. In vitro biocompatibility assessment comparing PVDF-HFP and PVDF-HFP-PPy membranes. Cell viability of a) murine embryonic fibroblasts (3T3) and b) human dermal fibroblasts after being exposed for 48 h to cell culture medium that was incubated for 24 h at 37 °C with either the PVDF-HFP or the PVDF-HFP-PPy membranes or control medium (mean \pm SD, N = 3). One-way ANOVA, where * p < 0.05, ** p < 0.01, *** p < 0.001, and n.s.; not significant (p > 0.05). The dashed line at 70% depicts the cytotoxic cut-off, based on EN ISO 10993-5.

2.5. Biocompatibility Evaluation

With the potential of using the superhydrophilic conductive PVDF-HFP-PPy electrospun membranes as a bio-interface material, we conducted a preliminary analysis of its biocompatibility. In vitro, cytotoxicity tests and qualitative analysis of cell morphologies can be used to evaluate the biocompatibility and cytotoxic properties of medical devices intended for direct contact with a patient's body. To assess whether any toxic substances leach from the membranes, both PVDF and PVDF-HFP-PPy membranes were incubated in cell culture medium for 24 h at 37 °C. Human dermal fibroblasts and murine embryonic fibroblasts were then treated for 48 h with either an untreated control medium or the medium that was exposed to the membranes. Qualitative morphological grading of the cells showed a slight response (defined as less than 20% of cells being rounded, according to EN ISO 10993) of cells that were exposed to the PVDF-HFP-PPy medium. Furthermore, a reduction in cell viability was observed in human dermal fibroblasts (Figure 4). However, this was less than 30%, the limit where a substance or medical device would be deemed toxic according to EN ISO 10993-5:2009.

3. Conclusion

There is a clear demand to streamline the development of intricate interface surfaces utilized across various fields. Our work presents a versatile and scalable approach for fabricating superhydrophilic, conductive nanoparticle-nanofibrous membranes. Unlike previous methods described in the literature, our platform enables the direct production of a superhydrophilic interface layer using hydrophobic nanofibrous membranes as the substrate, eliminating the need for post-modifications. The following key points underscore the significance in the field and advancements in biomaterial development demonstrated in this study:

- Simultaneous superhydrophilicity and conductivity:** This work establishes a novel approach for fabricating electrospun membranes that exhibit both exceptional superhydrophilicity and consistent high electrical conductivity, while upholding biocompatibility.
- Streamlined fabrication process:** The research offers a simplified and scalable strategy for the production of multifunctional membranes. The in situ synthesis eliminates the need for interface multi-layering, thereby significantly streamlining the device development process.
- Nanofiber-particle configuration:** The protocol describes a method of producing nanoparticle-decorated nanofibers, with the composite retaining its conductive and superhydrophilic properties even subsequent to vigorous washing and sonication.
- Amphiphilic Nature:** The fabricated membranes exhibit omniphilic behavior, showcasing an affinity for both polar and non-polar substances. This distinctive trait enables efficient interaction with a broad spectrum of analytes. Moreover, intergrating amphiphilic properties into PVDF membranes expands their applicability in diverse membrane research domains.
- Omnidirectional Conductivity:** The in situ fabrication method outlined herein yields composite membranes, in the form of a conductive sheet. This unique property facilitates efficient electrical charge transfer in all directions, rendering them highly suitable for diverse applications as a versatile interface platform.

The amalgamation of electrospinning with an intrinsically conductive polymer as a bulk synthesis route offers a valuable opportunity to establish a stable and versatile interface platform. Through this methodological approach, the study successfully generated membranes with a high affinity for both water and oil substances. The demonstrated capabilities of the produced and characterized composite membrane unveil new avenues for developing advanced materials with enhanced properties and functionalities. The developed platform has the potential for application in diverse fields, including energy, environmental monitoring, and biomedical diagnostics research, thereby presenting valuable opportunities for scientific and technological advancement.

4. Experimental Section

Materials: Poly(vinylidene fluoride-co-hexafluoro) co-polymer pellets (PVDF-HFP) (Mw \approx 400 000 Da, Mn \approx 130 000 Da), linear formula $(-\text{CH}_2\text{CF}_2)_x[-\text{CF}_2\text{CF}(\text{CF}_3)]_y$ were purchased from Sigma-Aldrich (USA) (product no. 427187). Pyrrole \geq 98%, iron(III) chloride hexahydrate ($\text{FeCl}_3 \cdot 6\text{H}_2\text{O}$), methanol (MeOH) 99.8% anhydrous, and acetone (AcOH) \geq 99.5% were obtained from Thermo Fisher Scientific (USA). Ethanol (absolute) 99.8% was purchased from Honeywell (UK). Sulfuric acid (H_2SO_4) 98%, phosphate-buffered saline (PBS) tablets (1X), N,N-dimethylformamide (DMF) 99.8%, Dihydrolevoglucosenone (Cyrene) \geq 98.5%, dimethyl sulfoxide (DMSO) anhydrous \geq 99.9%, and dimethyl carbonate (DMC) 99% were purchased from Sigma-Aldrich (USA). Deionized water was produced using Purelab Chorus 1 Complete water purification system (Elga LabWater, Veolia Water Systems LTD). Copper wire of 99.9% purity and 0.5 mm in thickness (CU510718) was acquired from Advent Research Materials (UK). Laminating pouches with a thickness of 250 microns were obtained from Fellowes Brands (USA), and the

silver-loaded conductive epoxy adhesive (RS-186-3616) was purchased from RS Components (UK). All chemicals were used as received.

Production of the PVDF-HFP Membranes: A conventional electrospinning setup was utilized to fabricate nonwoven nanofibrous membranes. Initially, 1.5 g of PVDF-HFP pellets were dissolved in 8.5 mL of a 7:3 (v/v) DMF:acetone mixture. The solution was magnetically stirred at ambient temperature until a translucent homogenous solution was obtained. The polymeric solution was then loaded onto a syringe and dispensed through a 21 G blunt needle (inner diameter 0.032 mm) at a constant rate of 15 $\mu\text{L min}^{-1}$ using a syringe pump. A potential difference of 21 kV (+15.5/-5.5 kV) was applied between the positively charged spinneret and a biased aluminum collector plate while jetting occurred from a 20 cm working distance. The fibers were collected onto a baking paper sheet for a batch duration of 4 h at a chamber temperature of 19–23 °C and relative humidity of 35%–50%.

As a green alternative fabrication method, similar nanofibrous membranes were produced under the same electrospinning parameters by dissolving 1.2 g of PVDF-HFP pellets in an 8.8 mL solvent system consisting of Cyrene: DMSO: DMC at a 3:3:4 (v/v) ratio. In this instance, the polymeric solution was magnetically stirred in an oil bath for 4–6 h at 70 °C until a homogenous golden solution was attained. In both cases, the electrospun membranes were vacuum-dried overnight at 40 °C.

In Situ Synthesis of Polypyrrole Particles on the Electrospun Membranes: Initially, the PVDF-HFP nanofibrous membranes were laminated into strips of 80 × 12 mm (outer) and 60 × 8 mm (inner, reaction site) to ensure a consistent surface area for polymerization. The pre-polymerization solution was prepared by homogenizing 1.8 M pyrrole in a 50/50 v/v mixture of ethanol and deionized water. The synthesis was adapted from established bulk chemical oxidative polymerization protocols previously described in literature.^[56–58] The mixture was sonicated for 15 min in an ultrasonic bath and magnetically stirred for 1 h at room temperature. Subsequently, the PVDF-HFP strips were immersed in the light-yellow in color pre-polymerization mixture and placed on a rocking platform shaker for 3 h, followed by ultrasonication for 15 min to allow for the entrapment of the monomer within the nanofibrous matrix. The immersion of the PVDF-HFP nanofibrous strips into the ethanol-based solution transformed the initially opaque white membranes into a translucent state (Figure S1, Supporting Information). Subsequently, the pre-soaked nanofibrous strips were transferred to a 0.2 M $\text{FeCl}_3 \cdot 6\text{H}_2\text{O}$ aqueous solution (oxidizing agent) and magnetically stirred for 24 h at 5 °C using a circulating chiller. The addition of pre-soaked nanofibrous membranes to the oxidizer induced a pronounced color change to black, indicative of the successful synthesis of polypyrrole. This was further affirmed by submerging non-pyrrole pre-soaked electrospun membranes in the oxidizing solution under the same conditions, which did not exhibit any color transformation (Figure S1, Supporting Information).

After polymerization, the membranes were washed twice in 10% v/v acetic acid and once in deionized water for 20 min, ultrasonicated for 10 min, and centrifuged for 5 min at 4000 rpm. The weight of the PVDF-HFP membranes prior to and post polypyrrole synthesis was also determined. Polypyrrole powder was synthesized following all the aforementioned steps, with the exception of omitting the PVDF-HFP membrane substrate.

Morphological Characterization: The pristine PVDF-HFP and composite particle-decorated electrospun membranes, as well as the PPy powder, were mounted onto aluminum stubs using carbon tape, evacuated overnight, and sputter coated with a 10 nm layer of gold using a Q150TS Plus sputter coater (Quorum, USA). Subsequently, high-resolution micrographs were obtained from an 8–10 mm working distance at a 5–15 kV accelerating voltage using the SU3900 scanning electron microscopy (SEM) instrument (Hitachi, Japan). High-resolution cross-sections were obtained by cutting the membrane using a scalpel, and subsequently following the aforementioned steps. Imaging of the cross-sections was performed using the JEOL JSM 7900F field-emission SEM (Jeol, Japan). The mean fiber diameter was computed using the Fiji-ImageJ software (v.1.53q, National Institutes of Health, USA). Three SEM micrographs were selected, and 180 fiber width values were measured per sample. Fiber diameter dis-

tribution histograms were also produced in SPSS (v.26, Statistical Package for Social Sciences, IBM, USA).

The pore size and pore size distribution were evaluated using capillary flow porometry with a Porolux 1000 instrument (IB-FT GmbH, Germany). The membrane thickness was measured using a digital caliper. The membrane porosity was determined gravimetrically by comparing the dry and wet membrane weights after wetting with a wetting agent (Porefil, IB-GT GmbH, Germany). The membrane porosity can be calculated using the following equation (Equation 1):

$$\% \text{Porosity} = \frac{W_{\text{wet}} - W_{\text{dry}}}{\rho \cdot A \cdot l} \times 100 \quad (1)$$

where W_{wet} and W_{dry} are the weights of the wet and dry membranes, respectively. A represents the area of the membrane, l is the thickness of the membrane, and ρ is the density of the wetting agent (1.87 g mL^{-1}).^[59]

Chemical Characterization and Wettability: Fourier-transform infrared spectroscopy (FTIR) was conducted using the attenuated total reflectance (ATR)-mode of an INVENIO-S spectrometer (Bruker, USA) and an iD7 Nicolet iS5 FTIR spectrometer (Thermo Fisher Scientific, USA). The spectra of the pristine materials and dried electrospun membranes were obtained by averaging 126 scans to improve the signal-to-noise ratio. Spectra were recorded at a spectral resolution of 1 cm^{-1} within the wavenumber range of 4000–400 cm^{-1} .

Elemental mapping of the nanofibrous surfaces was performed using energy-dispersive X-ray (ED) spectroscopy with a 170 mm² Ultim Max EDX detector (Oxford Instruments, UK) attached to the SEM. The obtained data were analyzed and interpreted using the AZtec software package.

XPS Analysis was performed using a Thermo NEXSA XPS fitted with a monochromated Al $K\alpha$ X-ray source (1486.7 eV), a spherical sector analyzer and 3 multichannel resistive plates, 128 channel delay line detectors. All data was recorded at 19.2W and an X-ray beam size of 400 × 200 μm . Survey scans were recorded at a pass energy of 200 eV, and high-resolution scans recorded at a pass energy of 40 eV. Electronic charge neutralization was achieved using a dual-beam low-energy electron/ion source (Thermo Scientific FG-03). Ion gun current = 150 μA . Ion gun voltage = 45 V. All sample data was recorded at a pressure below 10⁻⁸ Torr and a room temperature of 294 K. Data was analyzed using CasaXPS v2.3.19PR1.0. Peaks were fit with a Shirley background prior to component analysis. Lineshapes of LA(1.53,243) were used to fit components.

The water and oil wetting behavior of the vacuum-dried pristine PVDF-HFP and PPy particle-decorated electrospun membranes was assessed using a contact angle measurement system, OCA 25 (Data Physics, UK), at ambient temperature (19–23 °C). Orderly unswerving nanofibrous membranes ($n = 8$) were subjected to a 15 μL deionized water droplet or vegetable oil, and videos were recorded for analysis. The water contact angles (WCA) and oil contact angle (OCA) were measured using the contact angle add-on of the ImageJ software. The means \pm SD were calculated, and statistical analysis was performed using repeated measures ANOVA with Bonferroni's adjustment for confidence intervals in SPSS (Statistical Package for the Social Sciences v.28, IBM, USA). Supporting videos demonstrate the superhydrophilicity of the composite membranes compared to the pristine PVDF-HFP electrospun membranes.

The water retention of the pristine and composite membranes was evaluated based on Equation 2 below. Pre-weighed membranes (W_0) were placed in deionized water for 30 min. After immersion, the specimens were dried using Kimberly-Clark wipes and weighed again (W_i).

$$\% \text{Water retention} = \frac{(W_0 - W_i)}{W_0} \times 100 \quad (2)$$

Thermal Characterization: Thermograms were obtained to determine the onset of decomposition temperature (T_{onset}) of the PPy particle-decorated, pristine electrospun membranes and PPy powder via thermogravimetric analysis (TGA) using a SETSYS Evolution TGA instrument (Setaram, France). Each dried specimen weighing between 5–10 mg was placed on an open alumina crucible and heated from room temperature

up to 800 °C at a rate of 10 K min⁻¹ under argon atmosphere at an outlet pressure of 20 mL min⁻¹.

Four-Point Probe Measurements: Initially, the conductivity of the composite electrospun membranes was evaluated by measuring the sheet resistance using a four-point probe system: Jandel RM3000 (Jandel Engineering, UK). The RM3000 system consists of four equally spaced contacts with a probe spacing of ≈1 mm and can obtain readings ranging from 1 mOhm sq⁻¹ to 5 × 10⁸ Ohm sq⁻¹ with 0.5% accuracy. During measurement, the composite membranes were individually aligned directly beneath the probe head on the anodized aluminum base. The voltage was allowed to stabilize, and resistivity measurements were recorded. A total of six measurements were taken from two batches. The sheet resistance (Rs) was calculated using Equation 3 below, where *k* is the geometric factor for thin coatings (≈4.53), *V* is the voltage, and *I* is the current.

$$R_s = k \frac{V}{I} \quad (3)$$

Electrochemical Evaluation: For electrochemical analysis, the composite electrospun membranes were cut into 6 × 10 mm strips, and copper wire was used to create an electrode with silver-loaded conductive epoxy (thermal conductivity 11 W mK⁻¹). The silver epoxy was then cured at 60 °C for 2 h to establish the necessary electrical connection and provide mechanical stability. Next, the membranes were positioned in the center of 250 μm thick laminating pouches, with a 6 mm circular exposed area, and laminated to ensure a uniform testing area.

Cyclic voltammetry (CV) was conducted to study the electrochemical behavior and stability of the membranes. The measurements were carried out using a PalmSens4 potentiostat (PalmSens BV, Netherlands) equipped with a three-electrode setup and the PSTrace5 software. Stability assessment involved performing CV in a PBS pH 7.2 solution at a scan rate of 100 mV s⁻¹, within the potential range of 1.5 to -1.5 V (with a start and stop potential of 0 V) versus an Ag/AgCl electrode. A Pt wire (purity 99.95% and thickness 0.5 mm) served as the counter electrode. To examine the kinetic parameters, CV measurements were obtained for the same potential range at different scan rates: 500, 200, 100, 50, 20, 10, and 5 mV s⁻¹. Stability assessment involved subjecting the membranes to 100 CV cycles at a scan rate of 100 mV s⁻¹ in PBS electrolyte. As a comparative assessment this was performed before and after subjecting the membranes to a 24-h wash under constant magnetic stirring at 500 rpm, followed by a 30 min of sonication in an ultrasonic bath.

Battery-LED Visual Depiction: To visually demonstrate the conducting capability of the composite electrospun membranes in serving as a dry electrode to power a light-emitting diode (LED), a simple LED-9V battery circuit was assembled. The anode of the battery was affixed to the base of the membrane along with the short lead of the LED, while the cathode wire of the battery served as a switch, turning ON the LED upon contact with the top surface of the membrane.

In Vitro Biocompatibility Assessment: Adult human dermal fibroblasts were generously provided by the Walko lab, and murine 3T3 embryonic fibroblasts are from stock cultures from the Jungwirth lab. Cells were routinely subject to mycoplasma testing. All cells were cultured at 37 °C and 5% CO₂ in Dulbecco's Modified Eagle Medium (DMEM) supplemented with 10% fetal bovine serum (Merck F9665), 1% Penicillin/Streptomycin (Merck P4458), and 2 mM L-glutamine (Merck G7513). To test the effects of leachable substances from the membranes, 3 × 5 mm Ø PVDF-HFP or the PVDF-HFP-PPy membranes were incubated in 900 μL cell culture medium for 24 h at 37 °C and 5% CO₂.

For viability assays, 2–3 × 10⁴ cells well were seeded into 96-well plates 24 h prior to treatment. Cells were 60%–70% confluent when being treated with standard cell culture medium (control) or medium that was exposed to the two different membrane types for 48 h at 37 °C and 5% CO₂. Cell viability was measured using the EZMTT (MERCK, CBA411) assay kit according to the manufacturer's instructions. In brief, cell culture medium was removed, and 100 μL of 1:100 diluted EZMTT substrate were added per well and incubated at 37 °C for 2 h. The absorbance was measured at 450 nm using a BMG FLUOstar Omega (BMG Labtech, UK) plate reader.

Viability values were normalized to the viability of untreated cells, which served as negative control.

Supporting Information

Supporting Information is available from the Wiley Online Library or from the author.

Acknowledgements

This research received financial support from the UK Research and Innovation (UKRI) Engineering and Physical Sciences Research Council (EPSRC) Grant EP/V010859/1 and EP/V051083/1. The authors want to extend their gratitude to Prof Frank Marken for his early assistance in the electrochemical evaluation of the membranes. The authors acknowledge the Material and Chemical Characterization Facility (MC²) at the University of Bath (doi.org/10.15125/mx6j-3r54), Dr Philip Fletcher, and Dr Rémi Castaing for their expertise and assistance. X-ray photoelectron (XPS) data was acquired at the EPSRC National Facility for XPS ("HawellXPS", EP/Y023587/1, EP/Y023609/1, EP/Y023536/1, EP/Y023552/1, and EP/Y023544/1) and Dr David Morgan for quality assurance and assistance with data analysis and interpretation.

Conflict of Interest

The authors declare no conflict of interest.

Data Availability Statement

The data that support the findings of this study are available from the corresponding author upon reasonable request.

Keywords

conductive, electrospinning, nanofibers, nanoparticles, polypyrrole, PVDF-HFP, superhydrophilic

Received: January 14, 2024

Revised: March 18, 2024

Published online:

- [1] M. A. Hassan, N. N. Masnawi, N. Sultana, *ASAIJ*. **2018**, *64*, 415.
- [2] D. Chen, Z. Liang, Y. Liu, Z. Zhang, Z. Li, *Polym. Adv. Technol.* **2023**, *34*, 1451.
- [3] D. Zheng, L. Yang, W. Chen, Y. Fang, X. Wang, *ChemSusChem* **2021**, *14*, 3821.
- [4] T. Huo, F. Li, K. Jiang, W. Kong, X. Zhao, Z. Hao, Y. Pan, *ACS Appl. Nano Mater.* **2022**, *5*, 13018.
- [5] X. Wu, Z. Luo, Y. Lei, B. Wen, D. Yang, *Ind. Eng. Chem. Res.* **2020**, *59*, 21097.
- [6] S. Gupta, R. Datt, A. Mishra, W. C. Tsoi, A. Patra, P. Bober, *J. Appl. Polym. Sci.* **2022**, *139*, e52663.
- [7] R. Yu, H. Zhang, B. Guo, *Nanomicro. Lett.* **2021**, *14*, 1.
- [8] M. Waqas, A. Keirouz, M. K. Sanira Putri, F. Fazal, F. J. Diaz Sanchez, D. Ray, V. Koutsos, N. Radacsi, *Med. Eng. Phys.* **2021**, *92*, 80.
- [9] A. Keirouz, M. Chung, J. Kwon, G. Fortunato, N. Radacsi, *WIREs Nanomed. Nanobiotech.* **2020**, *12*, 1.

- [10] K. D. Patel, H.-W. Kim, J. C. Knowles, A. Poma, *Adv. Funct. Mater.* **2020**, *30*, 2001955.
- [11] S. Bhattacharya, I. Roy, A. Tice, C. A. Chapman, R. N. Udangawa, V. Chakrapani, J. L. Plawsky, R. J. Linhardt, *ACS Appl. Mater. Interfaces* **2020**, *12*, 19369.
- [12] H. L. Tan, M. K. Sanira Putri, S. S. Idris, N. Hartikainen, N. F. Abu Bakar, A. Keirouz, N. Radacsi, *J. Appl. Polym. Sci.* **2020**, *137*, 1.
- [13] M. Acosta, M. D. Santiago, J. A. Irvin, *Materials* **2022**, *15*, 8820.
- [14] R. Dallaev, T. Pisarenko, D. Sobola, F. Orudzhev, S. Ramazanov, T. Trčka, *Polymers (Basel)* **2022**, *14*, 4793.
- [15] W.-Z. Song, X.-X. Wang, H.-J. Qiu, N. Wang, M. Yu, Z. Fan, S. Ramakrishna, H. Hu, Y.-Z. Long, *Nano Energy* **2021**, *82*, 105695.
- [16] S. Ding, Z. Lyu, S. Li, X. Ruan, M. Fei, Y. Zhou, X. Niu, W. Zhu, D. Du, *Biosens. Bioelectron.* **2021**, *191*, 113434.
- [17] G. Anantha-Iyengar, K. Shanmugasundaram, M. Nallal, K.-P. Lee, M. J. Whitcombe, D. Lakshmi, G. Sai-Anand, *Prog. Polym. Sci.* **2019**, *88*, 1.
- [18] G. Veerappan, E. Ramasamy, B. Gowreeswari, in *Dye-Sensitized Solar Cells*, (Eds.: M. Soroush, K. K. S. Lau), Academic Press, US **2019**, 397.
- [19] A. Imani, G. Farzi, A. Ltaief, *Int. Nano Lett.* **2013**, *3*, 52.
- [20] T. H. Le, Y. Kim, H. Yoon, *Polymers (Basel)* **2017**, *9*, 150.
- [21] A. Omar, I. Goma, O. A. Mohamed, H. Magdy, H. S. Kalloub, M. H. Hamza, T. M. Mohamed, M. M. Rabee, N. Tareq, H. Hesham, T. Abdallah, H. Elhaes, M. A. Ibrahim, *Opt. Quantum Electron* **2023**, *55*, 381.
- [22] P. Zhang, R. Li, J. Huang, B. Liu, M. Zhou, B. Wen, Y. Xia, S. Okada, *RSC Adv.* **2021**, *11*, 11943.
- [23] S. Zhang, W. Tong, J. Wang, W. Wang, Z. Wang, Y. Zhang, *J. Appl. Polym. Sci.* **2019**, *137*, 48412.
- [24] H. Cheng, X. He, Z. Fan, M. S. Jeong, *Adv. Energy Mater.* **2019**, *9*, 1901085.
- [25] J. C. Barbosa, A. Fidalgo-Marijuan, J. C. Dias, R. Gonçalves, M. Salado, C. M. Costa, S. Lanceros-Méndez, *Energy Storage Mater.* **2023**, *60*, 102841.
- [26] M. Spasova, N. Manolova, N. Markova, I. Rashkov, *Fibers Polym.* **2017**, *18*, 649.
- [27] L. Zhou, C. L. Li, P. T. Chang, S. H. Tan, A. L. Ahmad, S. C. Low, *Desalination* **2022**, *527*, 115594.
- [28] S. Kim, J.-O. Jeong, S. Lee, J.-S. Park, H.-J. Gwon, S. I. Jeong, J. G. Hardy, Y.-M. Lim, J. Y. Lee, *Sci. Rep.* **2018**, *8*, 3721.
- [29] H. Bai, X. Wang, Z. Li, H. Wen, Y. Yang, M. Li, M. Cao, *Adv. Mater.* **2023**, *35*, 2211596.
- [30] Y. Zhu, W. Li, D.-Q. Yang, E. A. M. Sacher, *Surf. Interface Anal.* **2023**, *55*, 296.
- [31] A. L. McCaughey, P. Karandikar, M. Gupta, A. E. Childress, *ACS Appl. Polym. Mater.* **2020**, *2*, 1256.
- [32] S. Ramakrishna, V. J. Reddy, M. Fathi, M. Shamanian, A. Valipouri, *J. Biomed. Mater. Res. A* **2019**, *107*, 1154.
- [33] M. F. de Aguiar, A. N. R. Leal, C. P. de Melo, K. G. Alves, *Talanta* **2021**, *234*, 122636.
- [34] A. Keirouz, Z. Wang, V. S. Reddy, Z. K. Nagy, P. Vass, M. Buzgo, S. Ramakrishna, N. Radacsi, *Adv. Mater. Technol.* **2023**, *8*, 2201723.
- [35] J. Serra, L. C. Fernandes, N. Pereira, A. Fidalgo-Marijuan, J. M. Porro, C. Costa, D. M. Correia, S. Lanceros-Méndez, *ACS Appl. Polym. Mater.* **2022**, *5*, 109.
- [36] B. Dai, J. Fang, Y. Yu, J. Kou, H. Huang, C. Lu, Y. Zhao, Z. Xu, *Adv. Mater.* **2020**, *32*, 1906361.
- [37] S. Du, G. Ren, N. Zhang, X. Liu, *ACS Omega* **2022**, *7*, 19631.
- [38] A. Keirouz, Y. L. Mustafa, J. G. Turner, E. Lay, U. Jungwirth, F. Marken, H. S. Leese, *Small* **2023**, *19*, 2206301.
- [39] P. M. Shafi, R. Dhanabal, A. Chithambararaj, S. Velmathi, A. C. Bose, *ACS Sustain. Chem. Eng.* **2017**, *5*, 4757.
- [40] W. Liang, W. Yang, S. Sakib, I. Zhitomirsky, *Molecules* **2022**, *27*, 5313.
- [41] C. Dong, L. Xu, *ACS Appl. Mater. Interfaces* **2017**, *9*, 7160.
- [42] R. B. Keithley, P. Takmakov, E. S. Bucher, A. M. Belle, C. A. Owesson-White, J. Park, R. M. Wightman, *Anal. Chem.* **2011**, *83*, 3563.
- [43] G. Hussain, M. V. Sofianos, J. Lee, C. Gibson, C. E. Buckley, D. S. Silvester, *Electrochem. Commun.* **2018**, *86*, 43.
- [44] B. Saravanakumar, K. K. Purushothaman, G. Muralidharan, *ACS Appl. Mater. Interfaces* **2012**, *4*, 4484.
- [45] S. A. Fraser, W. E. van Zyl, *RSC Adv.* **2022**, *12*, 22031.
- [46] F. Aziz, L. Wlodarek, F. Alibhai, J. Wu, S. Li, Y. Sun, J. P. Santerre, R.-K. Li, *Adv. Healthcare Mater.* **2023**, *12*, 2203168.
- [47] Z. Liu, W. Wei, P.-L. Tremblay, T. Zhang, *Colloids Surf B Biointerfaces* **2022**, *220*, 112902.
- [48] L. Sun, Q. Gu, H. Wang, J. Yu, X. Zhou, *RSC Adv.* **2021**, *11*, 29527.
- [49] S. Malunavar, X. Wang, F. Makhlooghiyazad, M. Armand, M. Galceran, P. C. Howlett, M. Forsyth, *J. Phys.: Mater.* **2021**, *4*, 044005.
- [50] M. Khodamoradi, M. Eskandari, H. Keshvari, R. Zarei, *Mater. Sci. Eng., C* **2021**, *126*, 112180.
- [51] M. Wang, L. Wang, N. Deng, X. Wang, H. Xiang, B. Cheng, W. Kang, *Cellulose* **2021**, *28*, 6567.
- [52] D. K. Maurya, V. Murugadoss, S. Angaiah, *J. Phys. Chem. C* **2019**, *123*, 30145.
- [53] E. Číková, M. Mičušík, A. Šišková, M. Procházka, P. Fedorko, M. Omastová, *Synth. Met.* **2018**, *235*, 80.
- [54] B. Maharjan, V. K. Kaliannagounder, S. R. Jang, G. P. Awasthi, D. P. Bhattarai, G. Choukrani, C. H. Park, C. S. Kim, *Mater. Sci. Eng., C* **2020**, *114*, 111056.
- [55] V. K. Sharma, G. Chakraborty, S. Narendren, V. Katiyar, *Mater. Adv.* **2023**, *4*, 6294.
- [56] M. Yu, L. Wu, J. Miao, W. Wei, A. Liu, S. Liu, *Anal. Chim. Acta* **2019**, *1080*, 84.
- [57] S. P. Usha, A. M. Shrivastav, B. D. Gupta, *Biosens. Bioelectron.* **2017**, *87*, 178.
- [58] A. Mehdinia, M. O. Aziz-Zanjani, M. Ahmadifar, A. Jabbari, *Biosens. Bioelectron.* **2013**, *39*, 88.
- [59] M. Tang, K. S. S. Christie, D. Hou, C. Ding, X. Jia, J. Wang, *J. Memb. Sci.* **2021**, *617*, 118666.